Electronic Supplementary Material (ESI) for Chemical Communications.

Supporting information

Energy-resolved distribution of electron traps for O/S-doped carbon nitrides by reversed double-beam photoacoustic spectroscopy and the photocatalytic applications to Cr(VI) reduction

Chitiphon Chuaicham[a], Sekar Karthikeyan[a], Radheshyam R. Pawar[a], Yihuang Xiong[b], Ismaila Dabo[b], Bunsho Ohtani[c], Yoonyoung Kim[d,e], Jun Tae Song[d,e], Tatsumi Ishihara[d,e] and Keiko Sasaki[a,c]*

a. *Department of Earth Resources Engineering, Faculty of Engineering, Kyushu University, 744 Motooka, Nishiku, Fukuoka 819-0395, Japan, E-mail: keikos@mine.kyushu-u.ac.jp*

b. *Department of Materials Science and Engineering, The Pennsylvania State University, University Park, Pennsylvania 16802, United States*

c. *Institute for Catalysis, Hokkaido University, Sapporo 001-0021, Japan.*

d. *Department of Applied Chemistry, Faculty of Engineering, Kyushu University,*

744 Motooka, Nishiku, Fukuoka 819-0395, Japan

e. *International Institute for Carbon-Neutral Energy Research (I2CNER),*

744 Motooka, Nishiku, Fukuoka 819-0395, Japan

*Corresponding author: Keiko Sasaki,

E-mail: keikos@mine.kyushu-u.ac.jp

Tel & Fax: +81-92-802-3338

E-mail: chitiphon.c@gmail.com (C. Chuaicham)

1. Materials and reagents

Melamine, urea, thiourea, ammonium thiocyanate, and dicyandiamide were purchased from Wako Chemicals (Osaka, Japan). The structures of the precursors are shown in Fig. S1. All chemicals used were of pure analytical grade and were utilized without further purification. Ultrapure water was used in the preparation of the organic dye solutions and their subsequent experiments.

2. Synthesis of heteroatom-doped C_3N_4 by different precursors

The different heteroatom-doped C_3N_4 samples were fabricated by the thermal polymerization of various precursors. Melamine and dicyandiamide were used as precursors for the preparation of undoped C_3N_4. Urea and cyanuric acid were used as precursors for the preparation of O-doped C_3N_4, while thiourea and ammonium thiocyanate were used for the preparation of S-doped C_3N_4. In a typical preparation, exactly 5 g of each precursor was placed in a well-cleaned an alumina crucible with a cap and was then transferred into a muffle furnace. The furnace temperature was maintained at 550 °C for 2 h under the continuous flow of air. After complete calcination, the crucible was cooled down to room temperature. The obtained product from melamine, dicyandiamide, urea, cyanuric acid, thiourea, and ammonium thiocyanate were denoted as CMA, CDM, CU, CCA, CT, and CAT, respectively. Moreover, the calcination of melamine in the N_2 flow also was prepared and denoted as CMN.

3. Photocatalytic reduction of Cr(VI)

Photocatalytic activity tests were conducted on the photocatalytic reduction of Cr(VI). In a typical procedure, 12.5 mg of the different C_3N_4 samples and 1 mL of ethanol were added to 50 mL of 50 ppm of a $K_2Cr_2O_7$ solution in dark conditions for 10 min to establish the adsorption-desorption equilibrium. The initial pH of suspension was adjusted to pH 2 by 1 M HCl and 1 M NaOH. The suspensions were irradiated using a 500 W Xe lamp with a UV cut-off filter to provide the visible light. Then, the light source was turned on, and the photo reactor was cooled at 25° C throughout the reaction using a cooling circulator water bath. During the light illumination at different time intervals, the suspension was withdrawn with a syringe and filtrated through a 0.45 µm membrane to remove the solid samples. The remaining concentrations of $Cr_2O_7^{2-}$ were determined using a diphenylcarbarzide colorimetric method with an UV-vis spectrometry at 550 nm.

4. Characterization

The phase structure of synthesized C_3N_4 samples were investigated by XRD with an Ultima IV diffractometer (Rigaku, Akshima, Japan), using Cu Kα radiation with a 40 kV acceleration voltage and 40 mA applied current at a 2°/min scanning speed and 0.02° step size. The elemental compositions of undoped C_3N_4 and O/S-doped C_3N_4 were determined by XRF spectroscopy using Rigaku ZSX Primus II in the wavelength dispersive mode (Akishima, Japan). The functional groups of all synthesized C_3N_4 were characterized by FTIR with Jasco FTIR-670 Plus (Tokyo, Japan). The band gap energy of undoped C_3N_4 and O/S-doped C_3N_4 were estimated by using a Shimadzu UV-2450 spectrophotometer equipped with an ISR-2200 integrating sphere attachment (Kyoto, Japan). Electrochemical impedance spectroscopy (EIS) measurement was conducted by an electrochemical instrument in 0.5 M Na_2SO_4 electrolyte solution in single compartment quartz cell. A three-electrode cell system was applied with 10 mg of samples on FTO glass as the working electrode, Pt wire as the counter electrode, and Ag/AgCl in 3M NaCl as the reference. Solid state photoluminescence (PL) spectra of samples were measured using a JASCO F-6600 spectrofluorometer. Time-resolved photoluminescence (TRPL) spectra were measured on a Horiba, Fluoro Cube spectrophotometer laser wavelength at 295 nm.

5. RDB-PAS

Synthesized C_3N_4 samples of around 200 mg were added to a PAS cell equipped with an electret condenser microphone and a quartz window on the upper side under N_2 flow saturated with methanol vapor for at least 30 min. A light beam from an Xe lamp with a grating monochromator modulated at 80 Hz by a light chopper was irradiated from 650 nm to 350 nm through the cell window to detect the PAS signal using a digital lock-in amplifier. The ERDT were obtained by determining the amount of photo-absorption change for the accumulated electrons [1].

6. Calculation of total degree of coincidence

The overall degree of coincidence of the photocatalyst can be evaluated using the following equation:

$$\zeta = \zeta(a) * \zeta(b)^{\frac{1}{2}} * \zeta(c)^{2}, \tag{1}$$

where ζ(a) is the ERDT pattern matching (f) that was evaluated for two ERDT spectra f_s (ERDT-pattern profiles as a function of energy from VBT; integrated f is equal to the total density of ETs, D), f(1) and f(2) (D(1) < D(2)), as showed in Eqs. (2 and 3).

$$\zeta(a) = 1 - \frac{\int |f(1) - \alpha f(2)|}{\int f(1)} \left[\int f(1) < \int f(2)\right] \quad (2)$$

With α to minimize

$$\alpha: \int (f(1) - \alpha f(2))^2 \ (minimun) \quad (3)$$

ζ(b) is the total density of ETs (D) that was evaluated by the following equation:

$$\zeta(b) = \frac{D(1)}{D(2)} [D(1) < D(2)] \quad (4)$$

Moreover, ζ(c) is CBB Energy that was evaluated using the following equation:

$$\zeta(c) = \frac{CBB(1)}{CBB(2)} [CBB(1) < CBB(2)] \quad (5)$$

7. Calculation of degree of coincidence for photocatalytic reduction of Cr(VI)

The degrees of coincidence for photocatalytic reduction of Cr(VI), ζpc, of heteroatom-doped C_3N_4 samples were calculated using the following equation:

$$\zeta_{pc} = \frac{A(1)}{A(2)} [A(1) \leq A(2)] , \quad (6)$$

where A1 and A2 are the photocatalytic reduction of the Cr(VI) of different heteroatom-doped C_3N_4 samples when the value of A1 is higher than that of A2.

8. DFT calculation

To simulate doping in C_3N_4, we constructed a 2×2×1 supercell from the layered geometry with 15 Å of vacuum separating each layer to eliminate periodic image interactions. As shown in Fig. S2, we consider three symmetrically unique nitrogen atoms as possible substitution sites, namely, the center, edge, and connection nitrogen that are denoted N_{center}, N_{edge}, and $N_{connect}$, respectively. The electronic-structure calculations are performed at the PBE semi-local level of density-functional theory [2] using the projected augmented wave method implemented in the VASP [3]. The optimized Grimme-D2 pairwise force field is employed to account for the van der Waals interactions. The isolated C_3N_4 layer is constructed from a graphitic C_3N_4 crystal with space group $P\bar{6}m2$ by variable cell relaxation [4]. Structure optimization is carried out with the plane-wave cutoff of 520 eV, and the Brillouin zone is sampled with a 4×4×8 Monkhorst-Pack grid [5].

The local preference for oxygen and sulfur doping is evaluated by computing the energy of substitution:

$$\Delta E_X = E((C_3N_4)_{doped}) - E(C_3N_4) - \mu(X) + \mu(N), \qquad (7)$$

where X represents either S or O, $E(C_3N_4)_{doped}$ is the total energy of pristine C_3N_4, $E((C_3N_4)_{doped})$ is the energy of doped C_3N_4, and $\mu(X)$ and $\mu(N)$ are the chemical potentials of the doping elements and nitrogen atoms referenced to their elemental forms, respectively.

To address the known underestimation of the formation of the new electronic state after O/S doping, the hybrid Heyd-Scuseria-Ernzerhof functional (HSE06) [6] is employed, yielding the projected density of states (PDOS).

9. FTIR results

The FTIR spectra of C_3N_4 synthesized using the different precursors were presented in **Fig. 1b**. The FTIR spectra showed several characteristic peaks in the range of 1200 cm^{-1} to 1650 cm^{-1}, which can be assigned to C-N in a heterocycle stretching mode. The peaks at 1643 cm^{-1}, 1565 cm^{-1}, 1459 cm^{-1}, and 1411 cm^{-1} are attributed to the stretching vibration mode of heptazine ring.[7] The peaks at 1326 cm^{-1} and 1243 cm^{-1} correspond to the bending vibration mode of heptazine.[8] The representative peaks at 881 cm^{-1} and 809 cm^{-1} are assigned to the N-H deformation mode and tri-3s-triazine cycle skeletal bending mode, respectively.[9] The broad bands in a range of 2900–3500 cm^{-1} were ascribed to the O-H vibration mode of adsorbed H_2O molecules and the N-H vibration mode of the edge of the C_3N_4 sheet.[10] The expected stretching vibration mode of C-O-C and C-S-C in S/O doped C_3N_4 samples cannot be observed due to the low concentration of these functionalities.

10. TRPL and EIS results

The Time Resolved Photo-Luminescence (TRPL) decay curve give an essential information for lifetime of excited electrons, which is the key factor to determine the radiative recombination of photoinduced charge carriers. The PL lifetime of CCA photocatalyst showed the two emissive state with half-lives for 1.57 $\tau 1$/ns and 6.29 $\tau 2$/ns. The rapid decay factor ($\tau 1$) is related to inter-band exciton of radiative recombination emission, while the short decay factor ($\tau 2$) is related to indirect recombination radiative emissions from photo generated trapped electrons from holes in VB position.[11] From the biexponential decay curve, the CCA showed slower decay curve than other samples **(Fig. S6a,b and Table S5**), indicating that the O-doped C_3N_4 have longer lifetime of photogenerated electrons and slower radiative recombination of photoexcited electron-hole pairs, resulting to enhancing the photocatalytic activity.[12] Moreover, the electron transfers and charge separation of CCA (O-doped C_3N_4) and CAT (S-doped C_3N_4) were further studied using electrochemical impedance spectroscopy (EIS). It is clear that the CCA (O-doped C_3N_4) showed smaller radius of Nyquist circle compare with CAT (S-doped C_3N_4), indicating that the CCA might have high charge separation and electron transfer, corresponding to higher photocatalytic activity of CCA than CAT sample.

11. SSA results

The specific surface area (SSA) is one of the factors to enhance the photocatalytic activity due to enlarge the light absorption property and photogenerated electron-pair separation stabilized at the surface. Similar phenomena were observed in the doped C_3N_4 materials, exhibited outstanding surface area, textural properties, prolong lifetime of photo-induced charge carriers, and thereby contributing to the enhancement of overall photocatalytic activity in an aqueous phase.[13] Moreover, increasing of SSA by modification as well as doping of heteroatom in C_3N_4 enhance the light-harvesting ability and charge separation.[14, 15] SSA of the undoped and heteroatom doped C_3N_4 samples were 7.5 m^2g^{-1} (for CMN), 13.0 m^2g^{-1} (for CMA), 6.2 m^2g^{-1} (for CDM), 32.2 m^2g^{-1} (for CU), 73.9 m^2g^{-1} (for CCA), 9.5 m^2g^{-1} (for CT), and 10.6 m^2g^{-1} (for CAT), respectively. It is clear that the SSA of C_3N_4 materials increased after doping with heteroatoms (O or S). The O-doped C_3N_4 provide relatively higher SSA than S-doped C_3N_4 and undoped samples, in which the O-doped C_3N_4 are efficient photocatalytic Cr(VI) reduction.

Undoped C_3N_4	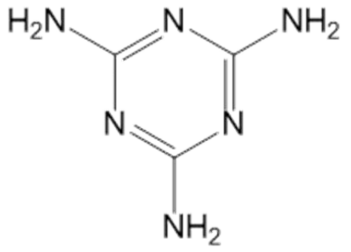 Melamine	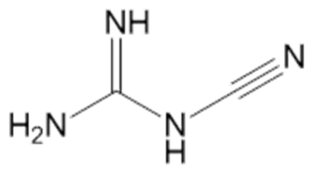 Dicyanamide
O-doped C_3N_4	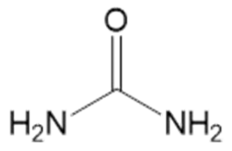 Urea	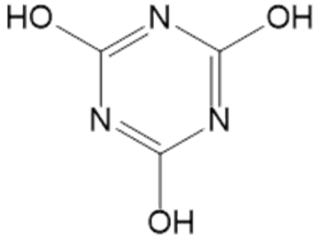 Cyanuric acid
S-doped C_3N_4	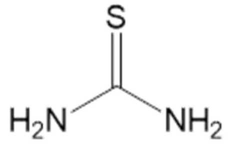 Thiourea	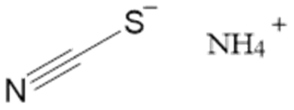 Ammonium thiocyanate

Fig. S1 Precursors for different heteroatom doped C_3N_4.

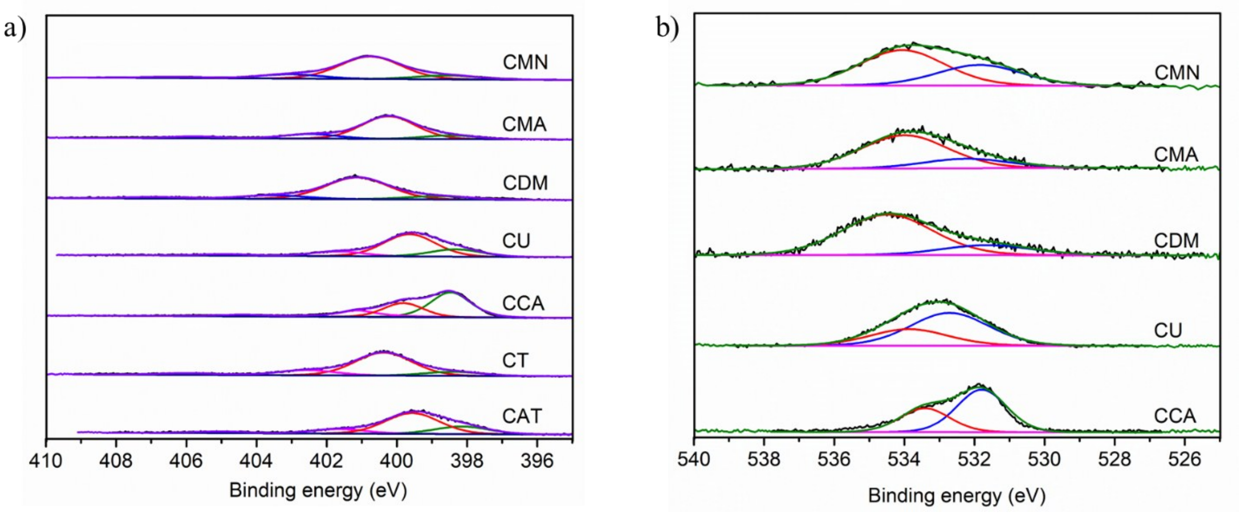

Fig. S2 XPS spectra of different heteroatom doped C_3N_4: a) N 1s and b) O 1s.

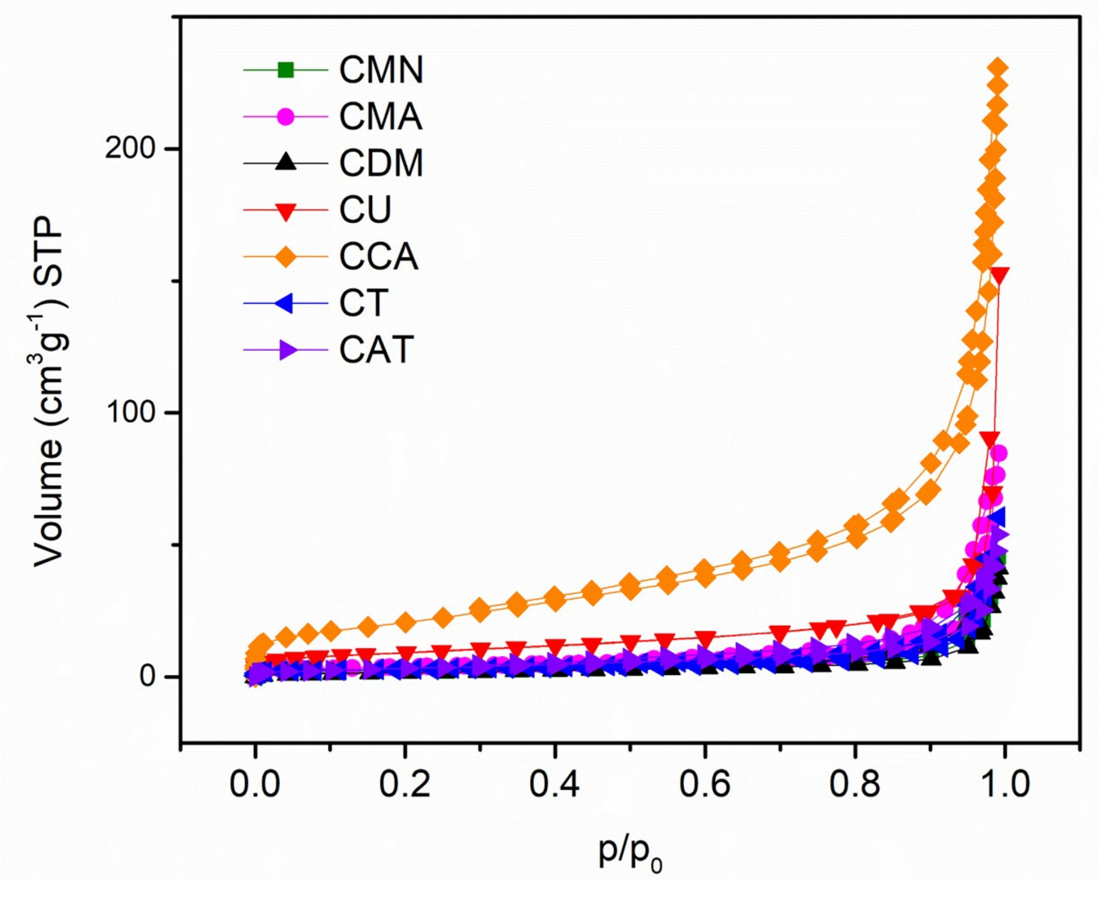

Fig. S3 N_2 adsorption and desorption isotherms of different heteroatom doped C_3N_4.

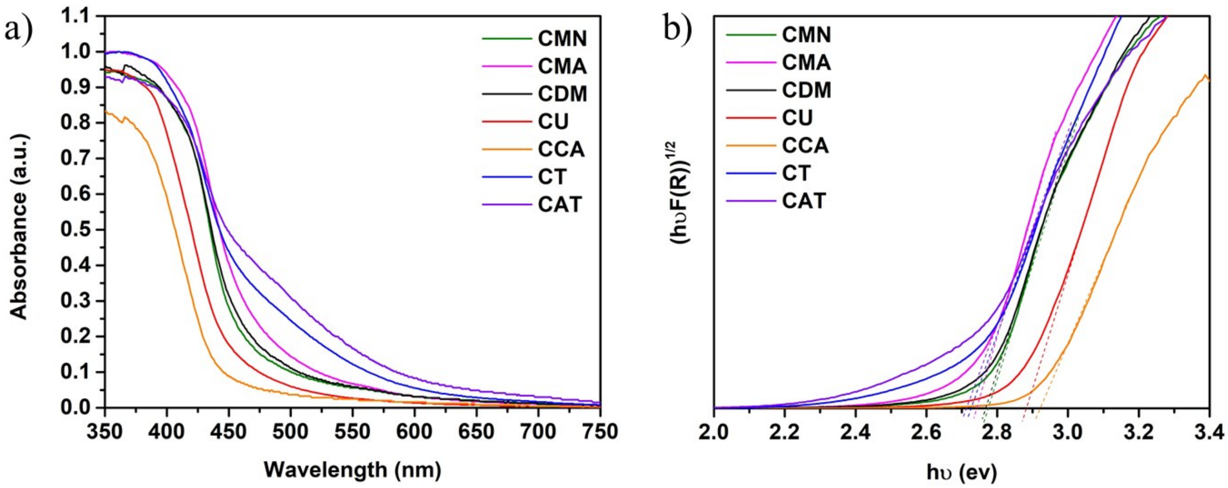

Fig. S4 a) DRS-UV spectra and b) corresponding Tauc plot of different heteroatom-doped C_3N_4.

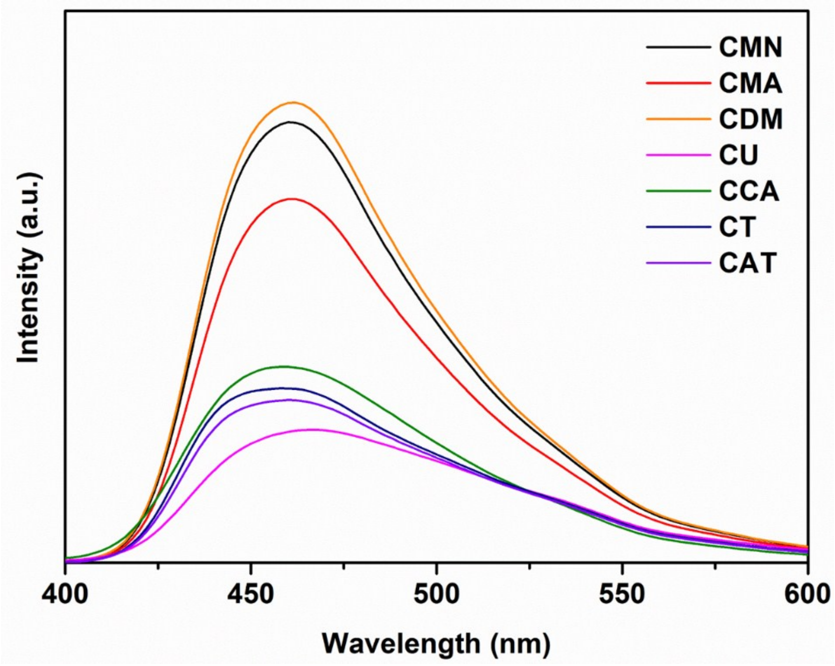

Fig. S5 Photoluminescence spectra of produced C_3N_4 from different precursors.

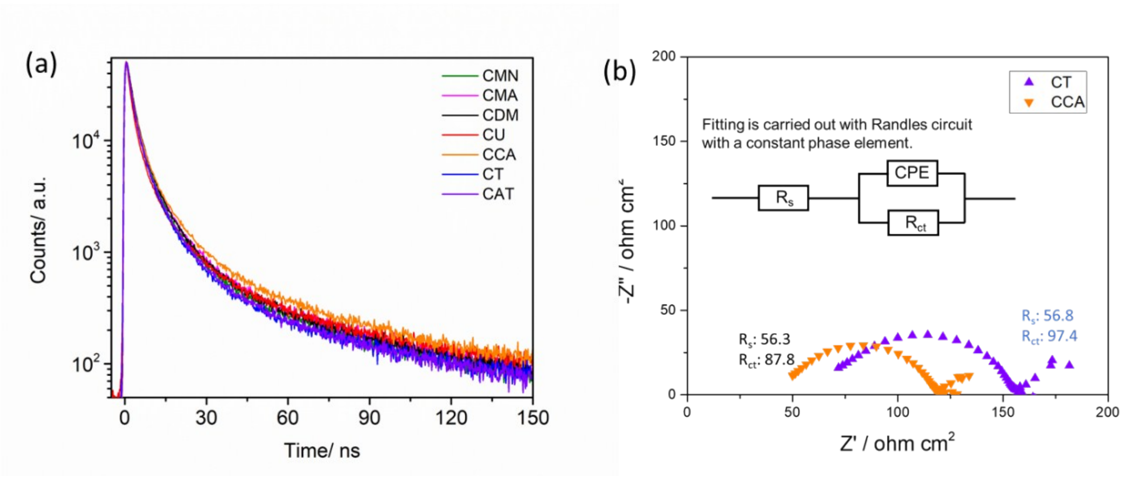

Fitting is carried out with Randles circuit with a constant phase element.

Fig. S6 a) TRPL of all samples and b) EIS spectroscopy of the CCA (O-doped C_3N_4) and CAT (S-doped C_3N_4).

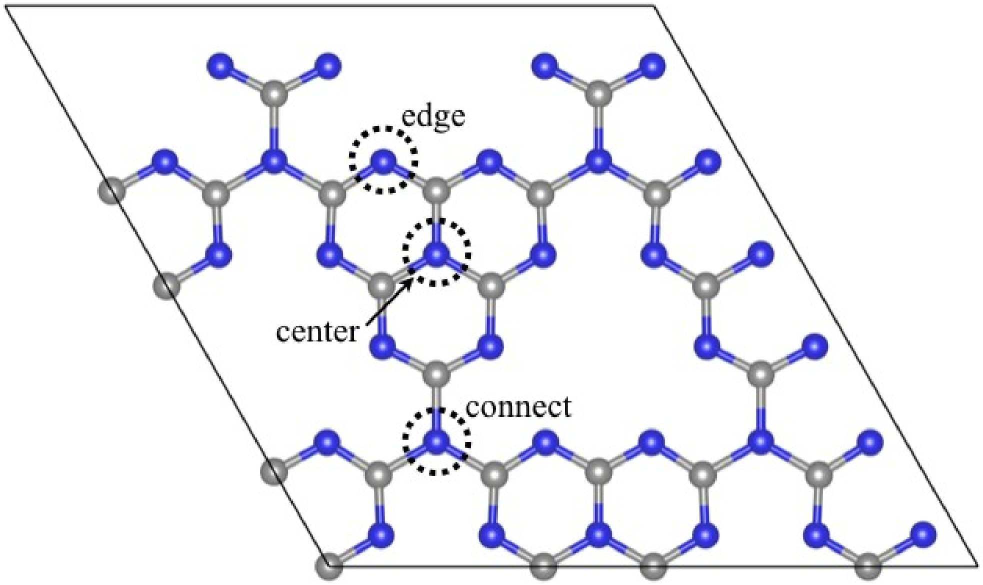

Fig. S7 Possible positions of sulfur and oxygen atoms to replace with nitrogen atoms in C_3N_4 at center (N_{center}), edge (N_{edge}), and connection ($N_{connect}$).

Table S1 Elemental compositions of different heteroatom doped C_3N_4 (wt%)

	C	N	O	S
CMN	27.38	72.62	-	-
CMA	27.84	72.16	-	-
CDM	27.74	72.26	-	-
CU	28.55	68.50	2.95	-
CCA	28.00	69.95	2.06	-
CT	28.05	71.84	-	0.11
CAT	27.45	72.49	-	0.06

Table S2 Surface molar ratio of O/N of undoped and O-doped C_3N_4.

	O/N ratio
CMN	0.03
CMA	0.04
CDM	0.04
CU	0.36
CCA	0.16

Table S3 SSA of different heteroatom doped C_3N_4

	SSA (m^2g^{-1})
CMN	7.5
CMA	13.0
CDM	6.2
CU	32.2
CCA	73.9
CT	9.5
CAT	10.6

Table S4 Degrees of coincidence for photocatalytic reduction in Cr(VI) and total degrees of coincidence of pairs of samples compared with CCA

	ζ	ζ_{pc}
CMN	0.37	0.59
CMA	0.35	0.59
CDM	0.43	0.59
CU	0.64	0.89
CCA	1	1
CT	0.29	0.64
CAT	0.31	0.66

Table S5 TPRL life time of doped and undoped C_3N_4 samples

	τ_1(ns)	**τ_2(ns)**
CMN	1.72	6.89
CMA	1.74	6.96
CDM	1.71	6.84
CU	1.74	6.96
CCA	1.97	7.90
CT	1.53	6.13
CAT	1.57	6.29

References

1. A. Nitta, M. Takase, M. Takashima, N. Murakami and B. Ohtani, *Chem Commun (Camb)*, 2016, **52**, 12096-12099.
2. J. P. Perdew, K. Burke and M. Ernzerhof, *Phys Rev Lett*, 1996, **77**, 3865-3868.
3. G. Kresse and J. Furthmuller, *Physical review. B, Condensed matter*, 1996, **54**, 11169-11186.
4. D. M. Teter and R. J. Hemley, *Science*, 1996, **271**, 53-55.
5. S. Grimme, *J Comput Chem*, 2006, **27**, 1787-1799.
6. H. J. Monkhorst and J. D. Pack, *Physical Review B*, 1976, **13**, 5188-5192.

7. K. Wang, Q. Li, B. S. Liu, B. Cheng, W. K. Ho and J. G. Yu, *Appl Catal B-Environ*, 2015, **176**, 44-52.
8. M. J. Bojdys, J. O. Muller, M. Antonietti and A. Thomas, *Chemistry*, 2008, **14**, 8177-8182.
9. J. Liu, Y. Liu, N. Liu, Y. Han, X. Zhang, H. Huang, Y. Lifshitz, S. T. Lee, J. Zhong and Z. Kang, *Science*, 2015, **347**, 970-974.
10. G. G. Zhang, J. S. Zhang, M. W. Zhang and X. C. Wang, *Journal of Materials Chemistry*, 2012, **22**, 8083-8091.
11. L. Xu, F. Zhang, X. Song, Z. Yin and Y. Bu, *Journal of Materials Chemistry A*, 2015, **3**, 5923-5933.
12. G. Katsukis, J. Malig, C. Schulz-Drost, S. Leubner, N. Jux and D. M. Guldi, *ACS Nano*, 2012, **6**, 1915-1924.
13. X. C. Wang, S. Blechert and M. Antonietti, *Acs Catalysis*, 2012, **2**, 1596-1606.
14. X. Wang, K. Maeda, X. Chen, K. Takanabe, K. Domen, Y. Hou, X. Fu and M. Antonietti, *J Am Chem Soc*, 2009, **131**, 1680-1681.
15. L. H. Lin, H. H. Ou, Y. F. Zhang and X. C. Wang, *Acs Catalysis*, 2016, **6**, 3921-3931.